IEEE Open Journal of
Industry Applications

Received 16 October 2025; revised 19 March 2026; accepted 20 April 2026. Date of publication 29 April 2026;
date of current version 13 May 2026.

Digital Object Identifier 10.1109/OJIA.2026.3688723

Minimizing Electromechanical Transients in Hydropower SEIGs: A Simple Approach for Smooth Islanded to Grid Synchronization

ANGELO ACCETTA [1] (Senior Member, IEEE), MASSIMILIANO LUNA [1] (Member, IEEE), MARCELLO PUCCI [1] (Senior Member, IEEE), MARCO SINAGRA [2], AND TULLIO TUCCIARELLI [2]

[1]Institute of Marine Engineering (INM), National Research Council of Italy (CNR), 153 90146 Palermo, Italy
[2]Department of Engineering, University of Palermo, 90128 Palermo, Italy

CORRESPONDING AUTHOR: ANGELO ACCETTA (e-mail: angelo.accetta@cnr.it).

This work was supported in part by the Ministero dell'Università e della Ricerca under Grant PNRR-M4C2, Grant ECS_00000022, in part by the title of research project: SiciliAn MicronanOTecH Research And Innovation CEnter SAMOTHRACE under Grant MUR, Grant PNRRM4C2, and Grant ECS_00000022, and in part by the spoke 3–Università degli Studi di Palermo S2-COMMs–Micro and Nanotechnologies for Smart & Sustainable Communities.

ABSTRACT This article addresses the management of electromechanical transients during disconnection and reconnection to the grid of turbine-driven induction generators (IGs) in hydraulic plants. Sudden loss of resistance torque after grid faults can lead to overspeed, mechanical stress, and potential water hammer effects. Conventional solutions rely on electric brakes and bypass valves to stop the IG and avoid damaging the whole mechanical and hydraulic system. When the grid is restored, to avoid severe torque and current transients, the IG must be reconnected as a motor in no-load conditions, the water flow is restored, and the machine starts operating as a generator. Such disconnection/reconnection transients result in long downtime even for brief faults. This article proposes a low-cost technique to avoid such complex and time-consuming procedures. The IG is not shut down but rapidly disconnected from the grid and operated as a self-excited induction generator (SEIG) using a capacitor bank while supplying a local resistive load. A steady-state analysis was performed to properly size passive components, ensuring the islanded SEIG operates near its grid-connected working point to enable smooth reconnection without expensive power converters. The proposed technique was tested in numerical simulation with a suitably devised space-vector dynamic SEIG model that is valid for both grid-connected and islanded operation, as well as experimentally using a dedicated test setup.

INDEX TERMS Self-excited induction generator (SEIG), low-cost energy harvesting, hydropower generation.

I. INTRODUCTION

Water distribution and transport networks have traditionally been designed only to meet consumer demands while keeping the pressure within a given range. Nowadays, however, the optimal design of hydraulic plants also involves exploiting the potential energy associated with the inlet flow rate [1].

Hydropower plants installed within aqueducts operate under fluctuating demand patterns, where flow rates change daily and seasonally. In such plants, an electric generator is mechanically coupled to the hydraulic turbine. Induction generators (IG) are frequently adopted since they can accommodate both mechanical and electrical variations with minimal control complexity, maintaining stable operation when directly connected to the grid. Their rugged construction, low maintenance requirements, and ability to operate efficiently in small to medium power ranges make them ideal for in-line turbines.

In these plants, an unexpected disconnection of the IG from the electrical grid in case of a grid fault can cause critical issues for both the hydraulic system and the generator. Although long periods of network failures are rare, transient faults are still very common. When a grid outage occurs, the IG is immediately disconnected from the grid so it loses active

and reactive power exchange with it. This leads to a sudden loss of electrical load while the turbine motoring torque on the shaft is still active. The abrupt loss of the resistance torque on the shaft can cause rapid speed increase of the turbine-generator unit, potentially resulting in overspeed, mechanical stress, and increased wear on rotating components. From a hydraulic perspective, the sudden change in torque can generate pressure transients and water hammer effects within the pipeline, threatening pipes, valves, and fittings. Therefore, proper protection systems (such as fast shut-off valves, bypass lines, and electrical protection relays) are essential to ensure safe operation and to maintain the aqueduct's primary function of reliable water distribution.

In detail, if a grid fault occurs, a proper command of actuators and valves is needed. In particular, an electric brake is needed to quickly stop the turbine rotor, and a bypass pipe including an auxiliary valve is needed to control head and/or discharge after the turbine stop. The electric power needed to supply such devices must be provided by an external power source, typically, an Uninterruptible Power Supply (UPS). The hydraulic plant downtime can consequently become very long (up to 30 min), even for very short failures of the power grid. Furthermore, even more problematic, when the grid is restored, the connection of the IG must be made as follows.

1) First, the IG is connected to the grid as a motor in no-load conditions.
2) Then, the water flow is restored, and the machine automatically starts operating as a generator working in the supersynchronous region.

Such a procedure is complex and very time consuming. Furthermore, the unregulated parallel connection of the IG to the power grid while receiving a motoring torque from the turbine is not allowed. In fact, severe torque and current transients would arise, potentially damaging the whole hydraulic and mechanical system.

The described complex and time-consuming procedure could theoretically be avoided if the IG is not shut down during a power grid failure. Instead, it could be rapidly disconnected from the grid and operated as a self-excited induction generator (SEIG) using a capacitor bank while supplying a local resistive load. Such passive components must be properly sized to make the SEIG operate closer to the grid-connected operating point, thereby guaranteeing a smooth reconnection transient.

Indeed, the easiest way to guarantee a smooth electromechanical transient during the reconnection to the grid is using a power converter to supply the machine. Such a choice is rarely accepted by the hydraulic network management agency, as it would introduce additional cost and complexity and reduce the overall reliability of the system.

An alternative solution is to conceive a direct parallel connection technology of the SEIG that minimizes the electromechanical transient occurring after the grid failure. This article addresses such a subject and proposes a low-cost technical solution, derived from *a priori* theoretical analysis and design.

II. RATIONALE FOR THE PROPOSED SOLUTION

To avoid the aforementioned expensive and bulky machinery, and the consequent long reconfiguration process, this article proposes a solution based on maintaining the regular work of the turbine even during the grid-failure condition. Aiming to propose a low-cost solution, the induction machine is supposed to be directly connected to the power grid, without any power converter, thus no control technique can be exploited to regulate the transient.

When the power grid is out of service, the IG works in an islanded configuration as an SEIG, and the produced power is exploited to supply a passive electric load. If no local load is present during the failure, the power is assumed to be dissipated in external resistors; alternatively, the excess power could be stored in a Battery Energy Storage System (BESS) for later reuse, as proposed in [2]. This procedure aims to keep the rotational velocity and the torque at the turbine shaft almost constant after the grid fault. In this configuration, the hydraulic machine continues to provide the pressure regulation, without potentially risky hydraulic transients for the water network or water flow interruption.

It should be noted that the electromagnetic transient between the grid-connected and the islanded configurations is not critical. The most critical issue is the correct *a priori* design of the capacitor bank and load resistance. In fact, if properly designed, such components permit the SEIG to work in an operating point that is as close as possible to the corresponding grid-connected operating point in terms of voltage amplitude and frequency. On the contrary, the electromagnetic transient from the islanded to the grid-connected configuration can be critical. If the instant at which the SEIG is directly connected to the power grid is not properly selected, a very severe electromechanical transient may occur, with high peaks of stator currents and electromagnetic torque that can damage both the IG and the turbine. The ideal connection instant occurs when grid and SEIG voltages are perfectly in phase. The situation is further complicated because, unlike the traditional procedure for synchronous generators, the SEIG is not connected to the grid as a generator in no-load conditions since the water flow is never interrupted in the proposed solution. Rather, the electrical power generated by the SEIG due to the torque applied by the turbine is immediately injected into the grid after the connection relay is activated.

Starting from the scientific literature, a steady-state analysis was conducted on the machine under test, ensuring the optimal design of the capacitance and load resistance values. Afterward, a space-vector dynamic model of the IG, including the excitation capacitors, was developed and expressed in state form. The model is valid for both grid-connected and islanded SEIG operation, allowing the analysis of transitions between the two working conditions. Finally, a low-cost technique was developed to implement smooth transitions between the above-cited working conditions. This technique was tested in numerical simulation based on the devised dynamic model and experimentally verified on a purposely devised test set-up. To the best of the authors' knowledge, no similar contribution has been found in the scientific literature.

It should be noted that the adoption of the proposed technique, besides providing technical advantages in terms of strong mitigation of the electromechanical transient, enables a significant reduction in the hydraulic plant downtime and lower costs by eliminating the need for certain devices. In fact, if the proposed technology is adopted, there is no need for an electric brake or valve, and therefore no need for a UPS providing additional power. The power needed to supply the controller board, the sensors, and the solid-state relay is provided by the electrical machine which, after the grid failure, starts operating as an SEIG in an operating point that is close to the grid-connected operating point. This article extends the work presented in [3] by improving the following aspects.

1) Recent scientific literature has been reviewed and included in the article.
2) A more in-depth theoretical analysis has been provided, covering both the steady-state and dynamic behaviour of the SEIG.
3) The design of the experimental setup needed to validate the proposed technique has been presented. Correspondingly, the experimental results have been presented and discussed in detail, whereas only preliminary simulation results had been shown in [3].

III. COMPARISON WITH THE SCIENTIFIC LITERATURE

There are several topics that are addressed in this article.

1) SEIG static and dynamic modeling.
2) Capacitor bank and load resistance design.
3) IG operation under grid fault.
4) IG-based hydropower plants.

While the scientific literature is rich of contributions on these topics, no contribution has been found that addresses all of them together, as done in this article. For this reason, the scientific literature review is organized in four sections, each focused on one of the abovecited topics.

A. SEIG STATIC AND DYNAMIC MODELING

Both the steady-state and dynamic analysis of the SEIG have been addressed in several papers in the scientific literature, from the 1980 s to the present. The pioneering work [4] presents a method for the steady-state analysis of SEIGs using balanced terminal capacitors. Operational and steady state equivalent circuits of the induction machine are employed to predict the steady state performance under different load conditions. Subsequent work [5] proposes a method based on nodal analysis, allowing the use of arbitrary functions for the torque–speed characteristic of the unregulated prime mover, to analyze the steady-state open loop behavior of the SEIG. Ion[6] presented a comprehensive overview of the literature dedicated to single phase IGs, focusing on several significant aspects such as main topologies, modeling, steady-state analysis, and performance investigations.

B. CAPACITOR BANK AND LOAD RESISTANCE DESIGN

The contribution presented in [3] shows that certain ranges of the machine speed, capacitance, and load resistance exist, where the SEIG can self-excite. In [7], it is shown that critical values of load impedance and speed exist, below which the machine fails to self-excite, regardless of the capacitance used. Chakraborty et al. [8] determined the speed limits for fixed terminal parameters and capacitance requirements under varying speeds and loads. In addition, they propose a method to test the possibility of self-excitation for known speed, load, and terminal capacitance. Finally, Haque[9] performs the steady-state analysis and assesses the performance of an isolated three-phase SEIG driven by a regulated or unregulated turbine.

Ojo and Jimoh [10] proposed simplified steady-state and dynamic performance analyses of an SEIG based on the system equations expressed in terms of the machine flux linkages. The contribution in [11] discusses the dynamic performances of an isolated SEIG under different power-factor loading conditions, where sudden connection and disconnection of various power-factor loads are investigated. More recently, Bansal [12] presented an exhaustive survey of the literature over the past 25 years, discussing the process of self-excitation and voltage buildup, modeling, steady-state, and transient analysis, reactive power control methods, and parallel operation of an SEIG. As a more recent contribution closer to the topic addressed, Singh et al.[13] presented a transient analysis of an SEIG with an electronic load controller (ELC) used in stand-alone micro-hydro power generation employing uncontrolled turbines. Consistently, Haque [14] proposed a genetic algorithm-based technique to estimate and analyze the steady-state performance of an SEIG, as well as an identification technique devised to achieve constant-voltage constant-frequency operation. The article [15] presented a simple method for analyzing the steady-state performance of an SEIG with $P - Q$ load model. Correspondingly, Teng et al. [16] proposed a reduced-order SEIG model with complex transformation in the two-phase stationary reference frame for the transient analysis of voltage build-up. Kiselychnyk et al. [17] developed a control-oriented linearized model written in the stator flux reference frame, which relates small deviations in capacitance, load admittance, and angular velocity to corresponding deviations in the voltage amplitude.

C. IG OPERATION UNDER GRID FAULT

Rao et al. [18] addressed the modeling of the IG and the analysis of the power system in case of different fault scenarios. As for the application of electric generation in hydraulic plants, the contribution in [19] discusses the design and implementation of a modified electronic load controller (MELC) for constant-frequency operation with voltage regulation of a two-winding single-phase SEIG for renewable energy applications, specifically for off-grid power generation based on a small-size hydrogeneration system. Kumar et al.[20] presented the design, development, and performance analysis of a three-phase synchronized ac chopper (SynACC)-based controller for small hydrogeneration systems. The three-phase SynACC-based controller is used to control the voltage and frequency of a three-phase SEIG-based small hydropower system. Fedor et al. [21] focussed on the development of

a functional simulation model of a small hydropower plant using an IG and to investigate the dynamics of fast electro–mechanical phenomena during individual start-up phases of the plant. Furthermore, they solve the problem of short-term voltage interruptions in the electrical network. Finally, Verma et al. [22] involved mathematical modelling and simulation to compare black start restoration capabilities of synchronous machines and doubly-fed induction machines-based hydro-generating units.

D. IG-BASED HYDROPOWER PLANTS

Olivo et al. [23] examined the main technologies that have been developed for mini-hydropower generators. A quick overview of hydraulic turbines and their energy characteristics is given, and different generator solutions are analyzed. The different technologies being considered include synchronous and induction machines, variable and fixed speed systems, grid-connected (direct-on-line) and converter-based solutions. An approach similar to the one adopted here is proposed in [24], where an uncontrolled hydraulic turbine is connected to an SEIG. In this application, the stator winding of the SEIG is connected to a PWM voltage source inverter (VSI), with a DC-link capacitor acting as a voltage source. In this case, the regulated frequency of the VSI ensures a constant frequency of the SEIG. From this point of view, this application guarantees a constant frequency operation of the SEIG, whereas the application proposed in this article does not. On the other hand, the advantage of the proposed approach is that no power converter is required, leading to a low-cost solution that meets the *a priori* requirements. A closer approach is presented in [25], where the unregulated steady-state behavior of a capacitor-excited three-phase IG in a stand-alone micro hydro power plant is predicted. Unlike the approach followed in this article, the standard equivalent circuit is converted into one with only parallel elements to reduce the complexity of the solution process, and only simulation results are presented.

IV. CASE STUDY

The chosen case study is the hydropower plant prototype that is available at the University of Palermo, Italy. The system is made up of a water pumping system and a test stand with the turbine prototype coupled with an IG connected to a resistive load. The pumping system provides the inlet pressure and the flow rate for the prototypal turbine. The system operates in closed-loop mode. It is composed of a water pressure booster pump unit, an open tank reservoir, a suction pipe, a supply pipe, a bypass pipe, a return pipe, and three manual valves, which allow for the regulation of both the flow rate and the pressure at the turbine inlet. The pressure booster unit has a pressure regulation range from to 6 bar, and an operation range from 5 to 50 Hz. The flow rate in the pumping system is measured by three flow meters installed in the suction, supply, and by-pass pipes. The turbine prototype is coupled to a generator, a torque-meter, and two digital manometers. The description of the test bench monitoring instrumentation system and the corresponding measurement error can be found in [7]. Fig. 1 shows the schematics of the adopted power plant, a detail of which is depicted in the photograph in Fig. 2, while Fig. 3 shows the capacitor bank used for the SEIG excitation. Finally, Fig. 4 shows the block diagram of the SEIG connection scheme, along with the block diagram of the proposed grid-connection algorithm, that is detailed in Section VI.

In the adopted test setup, the hydraulic power plant presents a rated power of 15 kW. This power rating is sufficiently high to represent, with a proper level of portability, hydraulic plants of much higher power rating, at least those present in Sicily (Italy), for which this application has been conceived. Table 1 shows a list of the rated values of the Sicilian hydro power plants. It can be observed that the rated powers are between 54 and 974 kW. There are no particular constraints limiting the application of the proposed technique up to these rated powers, as results from the following considerations.

1) The IG presents almost the same structure (squirrel cage configuration) up to the rated powers of the machines that can be adopted in the power plants of Table 1.
2) The solid state relay adopted in the test setup has a rated current of 25 A. However, solid state relays with similar turn-ON and turn-OFF times and higher rated currents are available on the market. They can be used at the rated power levels of the plants of Table 1.
3) The TI TMS320F28027 processor adopted for the software implementation can be used regardless of the rating of the hydraulic power plant, and the same considerations apply to the voltage sensors given that the hydroelectric plants under consideration are always connected to the low-voltage distribution network (230 V_{RMS}, 50 Hz in Europe).
4) The load resistance defining the operating point in SEIG operation can be properly designed and constructed (even with parallel/series combination) for any rating of the hydraulic plant.

V. STEADY-STATE AND DYNAMIC MODEL OF THE SEIG

A. STEADY-STATE ANALYSIS OF THE SEIG

The steady-state circuital inverse Γ model of the SEIG derived from [26] is shown in Fig. 5, where F is the angular frequency, V is the speed, R_s and R_r are the stator and rotor resistances, respectively, X_m, X_r, and X_σ the magnetizing, rotor, and global leakage reactances, and finally X_c is the external capacitance reactance. All the variables are expressed in p.u. (per-unit). The nodal admittance analysis presented in [8] and reproposed in the following, clearly shows that the working frequency of the SEIG, for given values of the machine speed and load resistance, is independent of the external capacitor reactance. In particular, the possible working frequencies F are the real solutions of the following 6th-order polynomial equation

$$A_6F^6 + A_5F^5 + A_4F^4 + A_3F^3 + A_2F^2 + A_1F^1 + A_0 = 0 \quad (1)$$

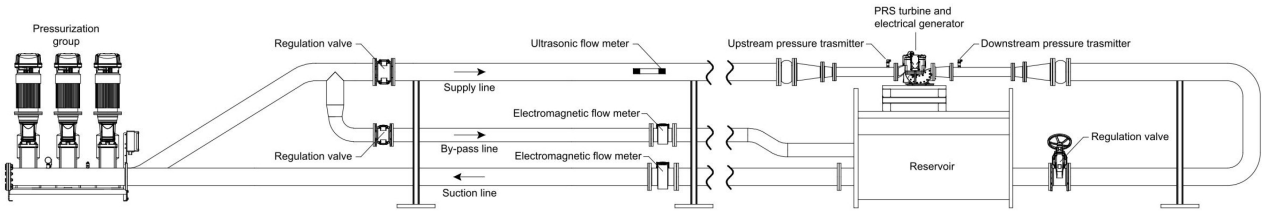

FIGURE 1. Schematic of the case study.

TABLE 1. Rated Values of the Sicilian Hydropower Plants

	Alcantara 1, Taormina (ME)	Blufi 1, Gela (CL)	Fanaco 1, Cammarata (AG)	Alcantara 2, Letojanni (ME)	San Giovannello, Trapani (TP)
Turbine type	Pelton	Pelton	Francis	Pelton	Cross-flow
Avg. flow rate (l/s)	470	200	420	220	130
Max flow rate (l/s)	600	250	600	300	180
Gross head (m)	209	336	42	231	42
Rated power (kW)	974	942	187	498	54
Avg. annual energy (kWh/year)	6,094,200	4,159,680	1,010,520	3,502,800	333,000

FIGURE 2. Photo of a detail of the case study.

TABLE 2. Polynomial Coefficients

parameter	value
A_6	0.0105
A_5	-0.0439
A_4	0.3208
A_3	-1.3439
A_2	1.0742
A_1	-0.2976
A_0	0.0088

FIGURE 3. Photo of the capacitor bank used for the SEIG excitation.

TABLE 3. SEIG Rated Values

Parameter	Value
rated power (kW)	15
rated speed (rpm)	1455
power factor	0.77
rated current (A)	29.8
I_s/I_n ratio	7.1
rated torque (Nm)	98.4
T_i/T_n ratio	2.4
T_b/T_n ratio	2.9
inertia $(kg \cdot m^2)$	0.0517

where coefficients A_i $(i = 0, \ldots, 6)$ depend on the IG parameters, its speed, and the load resistance; for their analytical expression as a function of the IG parameters, the reader can refer to the Appendix. Table 2 shows the coefficients A_i of the polynomial (1), for the IG under test, obtained at the selected operating point described later.

The SEIG under test is shown in Fig. 2, and its rated values are given in Table 3. Since the IG under test is mechanically connected to the hydraulic turbine, the traditional no-load

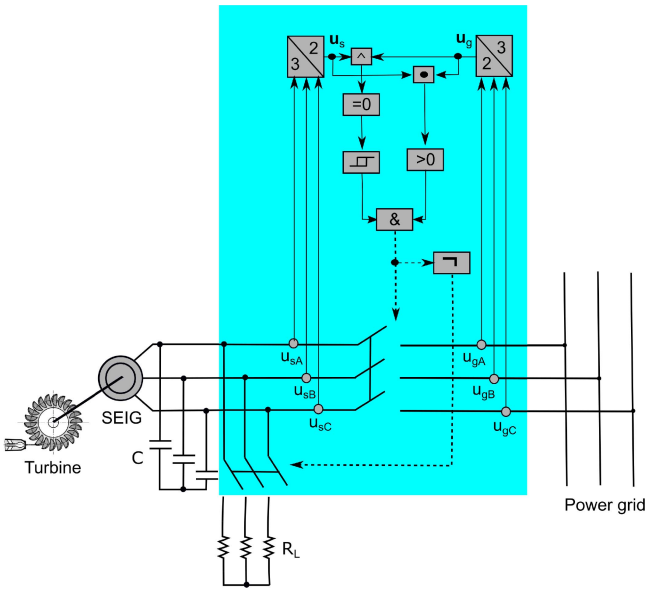

FIGURE 4. Block diagram of the SEIG connection scheme.

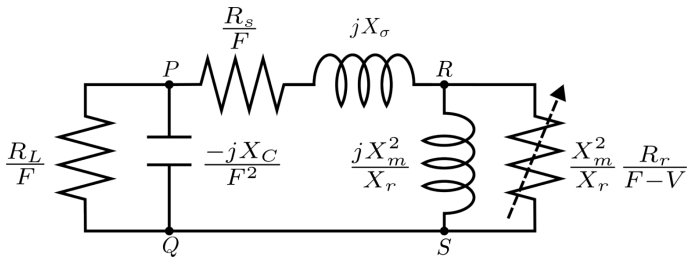

FIGURE 5. Steady-state circuit of the SEIG in p.u.

and locked rotor tests could not be exploited to measure the parameters of the T or Γ electric scheme. Since the IG is not supplied by a power converter, no other methodology based on the estimation of the machine parameters by the definition of proper voltage supply waveforms and related identification algorithms can be exploited. Under these constraints, it has been chosen to adopt a methodology that can identify the machine parameters using only the nameplate data [9]. The algorithm presented in [9] has been entirely programmed by the authors in MATLAB environment and then validated on other machines available in laboratory, with well-known parameters. Fig. 6 shows the surface describing the polynomial (1) versus the working frequency and the machine speed for the selected value of load resistance of 70 Ω. The same figure also shows the isolines corresponding to a null value of the polynomial, i.e., the real solutions of (1). Preliminarily, a possible working point in terms of working speed and working frequency in islanded operation has been selected as close as possible to the rated speed and grid frequency in grid-connected configuration. In the selected speed and load resistance ranges, the SEIG presents two possible branches (couples of frequency and speed), corresponding to the real roots of (1). In particular, the selected working point in islanded operation is identified

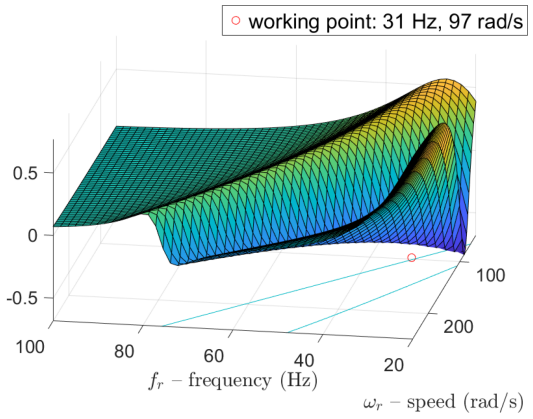

FIGURE 6. Surface describing (1) versus SEIG frequency and speed.

in Fig. 6 with a mark, corresponding to a working frequency of 0.62 p.u. (31 Hz) and a working speed of 0.63 p.u. (97 rad/s), obtained with a load resistance equal to 83.64 Ω.

It should be noted that the ideal working point would have been obtained with a load resistance of 6.5 Ω, which would have implied a working frequency of 1.02 p.u. (50.7 Hz) and a working speed of 1.10 p.u. (164 rad/s) [3]. Unfortunately, such a value of load resistance is not available in laboratory, therefore $R_L = 84\,\Omega$ has been selected as the load to be applied to the SEIG in case of grid failure. Such a load resistance R_L is connected to the SEIG only in case of power grid failure and then it is disconnected as soon as the IG is connected back to the power grid (see Fig. 4). The corresponding working point is obviously farther from the grid voltage operating point than the ideal one. From this point of view, demonstrating that the proposed technique works properly even with a nonideal resistance provides confidence that its behavior will be even better if the ideal SEIG working point is imposed, as shown in numerical simulation [3].

It can be further observed that, for the isoline branch under consideration, the relationship between the working frequency and working speed is almost linear, implying an almost constant slip speed. The nodal admittance analysis in [8] allows to determine the design value of the capacitance reactance. To this aim, the SEIG speed V must be selected, and the working frequency F must be determined as the largest solution of (1) for a given speed V (in this case, 31 Hz). According to [27], the formula to be used is

$$X_C = \frac{R_{\mathrm{PS}}^2 + X_{\mathrm{PS}}^2}{X_{\mathrm{PS}}} F^2 \tag{2}$$

where:

$$R_{\mathrm{PS}} = \frac{R_s}{F} + \frac{(F-V)\,R_r' X_m'^{\,2}}{R_r'^{\,2} + (F-V)^2\, X_m'^{\,2}}$$

$$X_{\mathrm{PS}} = X_\sigma + \frac{R_r'^{\,2} X_m'}{R_r'^{\,2} + (F-V)^2\, X_m'^{\,2}}$$

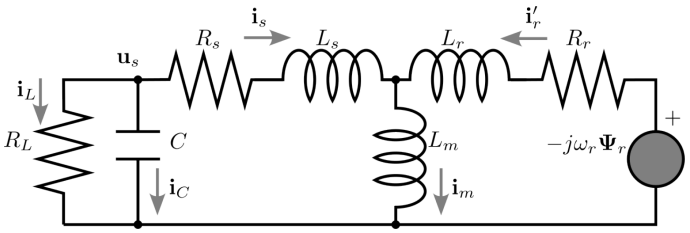

FIGURE 7. Space-vector circuit of the SEIG (stator reference).

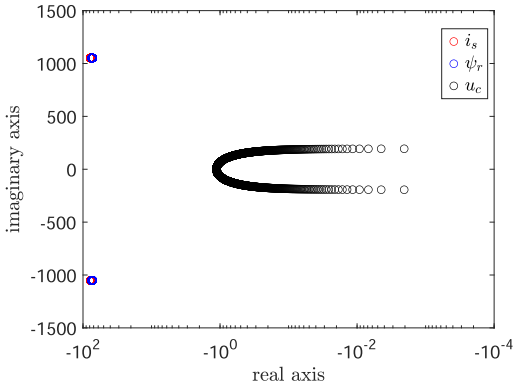

FIGURE 8. Eigenvalues of matrix A of the state-space model.

and $R'_r = (\frac{X_m}{X_r})^2 R_r$, $X'_m = \frac{X_m^2}{X_r}$. As for the SEIG under test, the design capacitance chosen according to (2) and used in the experimental system is equal to 200 μF. Once the SEIG has been designed in terms of capacitance and load resistance, it has been further verified that the working speed imposed by the turbine is higher than the minimum value permitting the self-excitation of the machine, which is equal to 13.1 rad/s, obtained as

$$\omega_{\min} = \sqrt{\frac{4\left[\tau^2 + \tau\left(K_1 + K_2\right) + K_1 K_2\right]\left(X_r X_\sigma + X_m^2\right) X_\sigma X_r}{X_m^2}} \tag{3}$$

being

$$K_1 = \frac{\left[R_s + R_r\left(\frac{X_m}{X_r}\right)^2\right]}{X_\sigma}$$

$$K_2 = \frac{R_s X_r}{X_r X_\sigma + X_m^2}$$

$$\tau = \frac{X_c}{R_L}.$$

In steps, the procedure to choose the load resistance and the capacitance values is the following.

1) First, the value of the load resistance is found by selecting a suitable working point of the SEIG in islanded operation (amplitude and frequency of the stator voltage close to the grid voltage) according to the locus of the solutions of (1).
2) The capacitance value is then computed according to (2).
3) The self-excitation capability of the SEIG is verified by computing the minimum working speed according to (3).

B. DYNAMIC ANALYSIS OF THE SEIG

As a first step, the dynamic model of the SEIG including the excitation capacitance has been written and expressed in state form. Such a model has been written starting from the space-vector circuit model of Fig. 7, expressed in the stator reference frame. It has been deduced assuming the following space vectors as the electric state variables: the stator current $\mathbf{i}_s$, the rotor flux $\boldsymbol{\Psi}'_r$, and the capacitance voltage $\mathbf{u}_c$. Such a formulation permits the straightforward analysis of the SEIG stability. The final space-vector state representation of the model is the following:

$$\begin{aligned}
\frac{d\mathbf{i}_s}{dt} &= -\left(\frac{1}{(\sigma T_s) + \frac{(1-\sigma)}{(\sigma T_r)}}\right)\mathbf{i}_s + \left(\frac{(1-\sigma)}{(\sigma L_m)}\right) \\
&\quad \left(\frac{1}{T_r} - j\omega_r\right)\boldsymbol{\Psi}'_r + \frac{1}{(\sigma L_s)}\mathbf{u}_c, \\
\frac{d\boldsymbol{\Psi}'_r}{dt} &= \frac{L_m}{T_r}\mathbf{i}_s - \left(\frac{1}{T_r} - j\omega_r\right)\boldsymbol{\Psi}'_r, \\
\frac{d\mathbf{u}_c}{dt} &= -\frac{1}{C}\mathbf{i}_s - \frac{1}{(R_L C)}\mathbf{u}_c.
\end{aligned} \tag{4}$$

In particular, the first equation in (4) represents the dynamics of the stator current; the second equation represents the dynamics of the rotor flux, whereas the third represents the dynamics of the capacitor voltage. The dynamic equation of the motion is

$$t_e = t_L + J_m\frac{d\omega_r}{dt} + B\omega_r \tag{5}$$

where t_L is the turbine torque. Such a quantity depends on the IG speed by a simplified law of the type

$$t_L = -\frac{\gamma Q \Delta H \eta_H}{\omega_r} \tag{6}$$

(minus sign because the motor convention is adopted), where γ is the water-specific weight, Q is the flow rate, ΔH is the head drop, and η_H is the turbine efficiency. Fig. 8 shows the poles of the SEIG, corresponding to the eigenvalues of matrix $\mathbf{A}$ of the state representation in (4) versus the SEIG speed, drawn for the selected values of C and R_L. The three branches related to the dynamics of the stator current, the rotor flux, and the capacitor voltage are recognizable. The fastest dynamics are those of the stator current and the rotor flux, followed by that of the capacitor voltage. It can be further observed that all three branches lie in the left half plane, confirming a stable behavior of the SEIG for the selected values of C and R_L. Finally, the poles related to the capacitor voltage lie quite close to the imaginary axis, as expected.

VI. TECHNIQUE FOR MINIMIZING THE ELECTROMECHANICAL TRANSIENT

The technique described in the following has been conceived for minimizing the electromechanical transient occurring during the transition from the islanded to the grid-connected configuration, which is the most stressful commutation, as previously explained. Such a technique is inspired by the logic underlying the connection of alternators in parallel with the power grid, although the SEIG is not in no-load conditions before grid connection, as stated in Section II. The electromechanical transient is caused by the vector difference $\mathbf{u}_g - \mathbf{u}_s$ between the space vectors of grid voltage $\mathbf{u}_g$ and SEIG voltage $\mathbf{u}_s = \mathbf{u}_c$. To minimize the electromechanical transient occurring when the SEIG is connected back to the power grid, following three conditions must be satisfied.

1) The difference between the SEIG and power grid frequencies must be minimum.
2) The difference between the SEIG and power grid voltage amplitudes must be minimum.
3) The difference between the SEIG and power grid voltage angles must be minimum.

Conditions 1) and 2) can be satisfied by properly designing the system. In particular, if the load resistance is suitably chosen, the SEIG working frequency (the maximum one) can be sufficiently close to the grid frequency, as shown in [3]. However, the SEIG frequency must be very close to the power grid frequency, but not exactly equal; otherwise, the methodology cannot be adopted as clarified in the following. If the SEIG capacitance is suitably chosen, its voltage amplitude can be sufficiently close or possibly equal to the grid voltage amplitude, since the working magnetic flux of the SEIG is close to the rated one. Condition 3) is critical: if the SEIG is closed in parallel with the power grid when the voltage angle difference is large, the IG draws a huge current with consequent torque, flux, and speed oscillations that can damage the machine and the connected turbine. To minimize the transient, then, the SEIG should be connected back to the power grid when the SEIG and grid voltages are in phase. To retrieve this working condition, the vector product between the SEIG and the power grid voltages is computed; in particular, the SEIG is connected back to the power grid when the vector product is null and the scalar product is positive (a necessary condition to ensure that the IG and grid voltages are in phase and not in counter-phase). The block diagram of the adopted technique is shown in Fig. 4. Both the SEIG and the three-phase grid voltages are sensed, and the related signals are acquired by a microprocessor. Such voltages are converted from the three-phase to the two-phase sD, sQ system in the stationary reference frame. Afterward, the vector and scalar products between these two voltage vectors are computed; when the ideal condition is reached, a command signal can be given to activate the grid connection relay, and the complementary signal disconnects the resistor bank. In practical applications, measurements from sensors are affected by noise, which can generate undesired and repeated commutations of the relay. To avoid such a problem, the hysteresis comparator in Fig. 4 (within the cyan rectangle) has been employed. The hysteresis band has been chosen equal to 0.05 after an offline analysis of the phase voltage measurements. The whole algorithm can be easily implemented on a low-cost embedded platform. It should be noted that the grid frequency is not measured in the proposed system. Only the instantaneous measurements of the grid and IG phase voltages are needed.

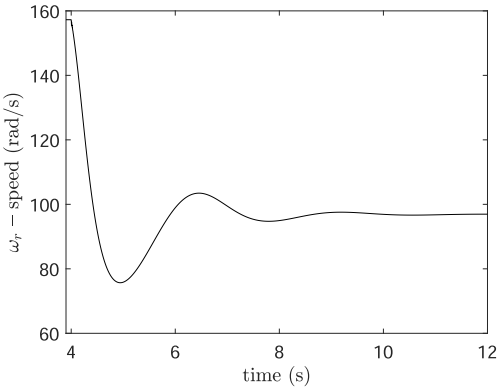

FIGURE 9. IG speed - transition from grid connected to islanded operation - SIMULATION.

VII. SIMULATION RESULTS

The proposed technique has been tested both in numerical simulation and experimentally. For the numerical simulation, the dynamic model of the entire system described by the set of space-vector equations (4) was implemented in the MATLAB-Simulink environment. The electrical parameters of the IG shown in Table 3, estimated on the basis of the methodology proposed in [9], have been adopted.

The system has been tested in following two working scenarios.

1) A failure of the power grid is simulated, making the IG work in islanded operation closed on a load resistance equal to 84 Ω (IG to SEIG).
2) A power grid restoration is simulated by reconnecting the SEIG, initially supplying a load resistance of 84 Ω, to the grid (SEIG to IG).

Both transitions are simulated to verify the transient behavior of the SEIG, its initial and final steady-state working points, and to validate the simulation environment against the experiments. Fig. 9 shows the speed of the IG during the transient from the grid-connected to the islanded operation, occurring at $t = 4$ s. The speed of the IG, equal to 150 rad/s in grid-connected operation, becomes equal to 95 rad/s in islanded operation, in agreement with the theoretical analysis in Section V.

Fig. 10 shows the rotor flux amplitude and the electromagnetic torque transients. It can be noted that rotor flux amplitude is very close in islanded and grid connected operation, slightly decreasing during the transient. The electromagnetic torque, after a transient with peak values of 280 N/m, equals the turbine torque at steady state, as expected.

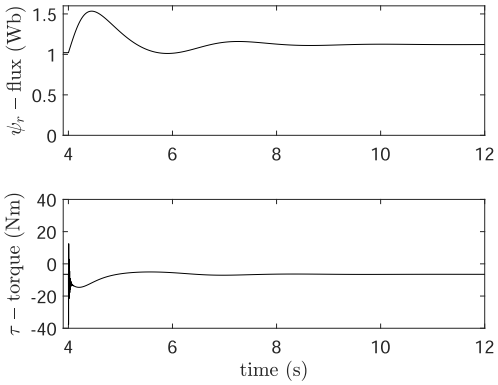

FIGURE 10. IG rotor flux amplitude and electromagnetic torque - transition from grid connected to islanded operation – SIMULATION.

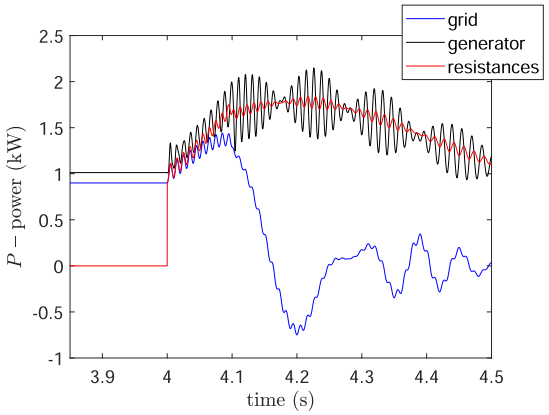

FIGURE 12. IG, load, and grid active powers - transition from grid connected to islanded operation – SIMULATION.

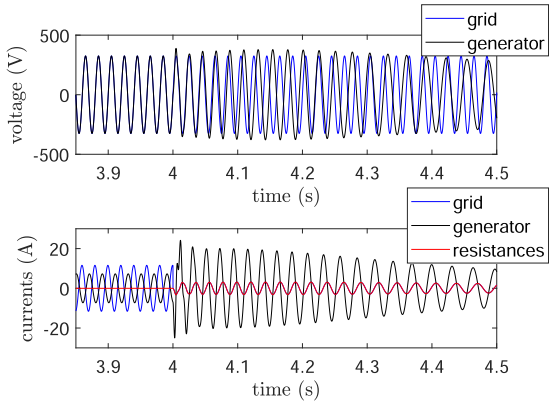

FIGURE 11. IG and grid voltages and IG, load, and grid currents - transition from grid connected to islanded operation – SIMULATION.

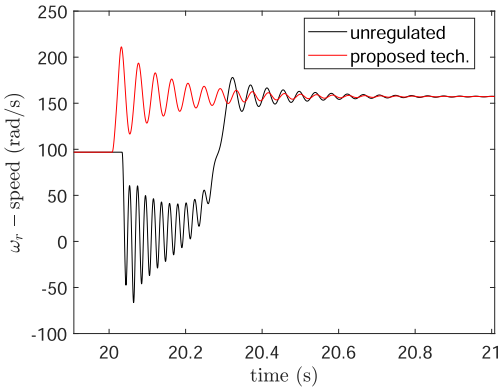

FIGURE 13. IG speed – transition from islanded operation to grid connected - SIMULATION.

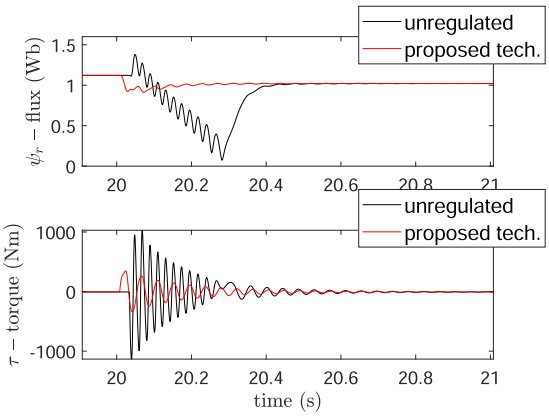

FIGURE 14. IG rotor flux amplitude and electromagnetic torque – transition from islanded to grid connected operation – SIMULATION.

Fig. 11 shows the grid and IG voltages, as well as the IG, the grid, and the load currents. It can be observed that, while the grid and IG voltages are equal during grid-connected operation, they tend to differ slightly in both amplitude and frequency in SEIG operation, as expected. In particular, the SEIG voltage amplitude is slightly lower than the grid voltage, and the working frequency becomes equal to 31 Hz. The IG currents reach values up to 25 A during the transient while settling to a steady-state value of 8 A, close to the corresponding value in grid-connected operation (7.5 A). It should be further noted that the IG current in SEIG operation differs from the load current because of the capacitor current. Fig. 12 shows the IG, load, and grid powers. It can be noted that the IG power, equal to the grid power during grid connection, becomes equal to the load power in SEIG operation.

Figs. 13–18 show the corresponding waveforms during the transient from islanded to grid-connected operation. In this case, the test was performed twice: once in an uncontrolled way (the commutation instant is random, and therefore its impact on the reconnection transient varies) and once in a controlled way, adopting the methodology proposed in this article. It can be observed that all the electrical variables vary in the opposite direction compared to the IG to SEIG transient. In particular, the rotor flux slightly increases, the voltage amplitude increases, and its frequency becomes equal to 50 Hz. The generator power, initially equal to the load power, becomes equal to the grid power at steady state.

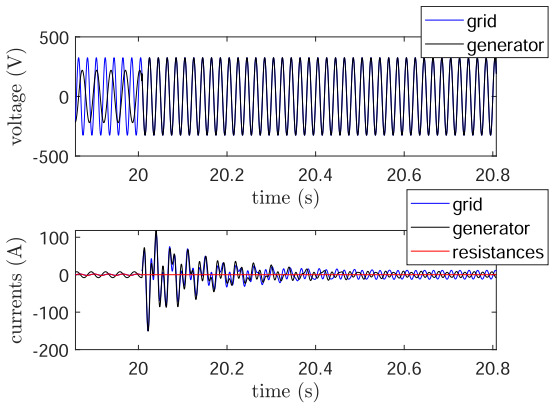

FIGURE 15. IG and grid voltages and IG, load and grid currents – regulated transition from islanded to grid connected operation – SIMULATION.

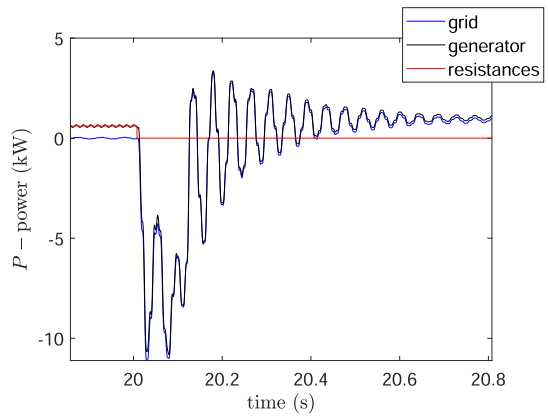

FIGURE 16. IG, load and grid active powers – regulated transition from islanded to grid connected operation – SIMULATION.

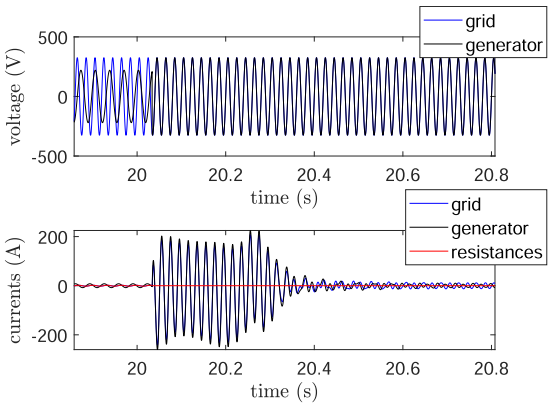

FIGURE 17. IG and grid voltages and IG, load and grid currents – unregulated transition from islanded to grid connected operation – SIMULATION.

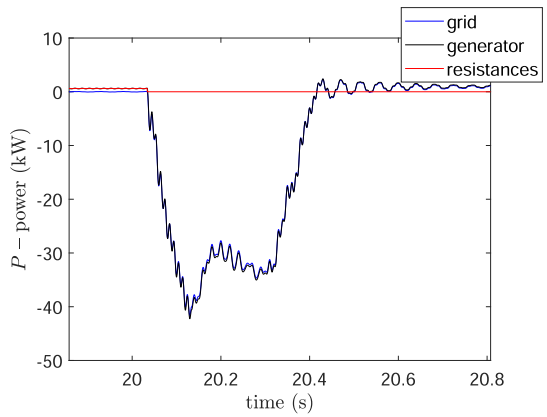

FIGURE 18. IG, load and grid active powers – unregulated transition from islanded to grid connected operation - SIMULATION.

These figures clearly show the advantages arising from the adoption of the proposed methodology with respect to a random connection to the power grid. In particular, with the proposed approach, passing from the SEIG to the grid-connected operation, the speed waveform presents a very smooth increase, and the rotor flux amplitude stays almost constant while transient torque does not exceed 200 N·m. On the contrary, with a random commutation instant, the speed presents a strong decrease close to zero, the machine demagnetises almost completely in transient, and the electromagnetic torque gets close to 1000 N·m in transient operation. Finally, Fig. 19 shows the current loci, $i_{sQ} - i_{sD}$ in the stationary reference frame, obtained during this transient with the proposed approach and with the random commutation. It can be clearly noted that the peak value of the stator current obtained during the transient with the proposed approach is much lower, 100 A versus 300 A. The advantages arising from the adoption of the proposed technique are clearly highlighted in Table 4. In this table, the following metrics are reported: the maximum value of the transient torque, the ratio between the maximum transient torque and the average torque, the integral absolute error (IAE) of the transient torque referred to its average value, the minimum value of the transient rotor flux, the ratio between the minimum transient rotor flux and the average rotor flux, and the IAE of the transient rotor flux referred to its average value. It can be observed that all these indexes are significantly improved with the proposed technique than without it.

TABLE 4. Quality Indexes for Simulation Tests - Islanded to Grid Transient

	Proposed solution	Unregulated
max torque (Nm)	346	1133
max-to-average ratio	53	174
torque IAE	41	99
min flux (Wb)	0.91	0.07
min-to-average ratio	0.89	0.07
flux IAE	0.02	0.17

VIII. EXPERIMENTAL SETUP & RESULTS

A. EXPERIMENTAL SETUP

The experimental test set-up is the hydropower plant prototype installed at the University of Palermo, Italy, which is sketched in Fig. 1 and described in Section IV. It is made up

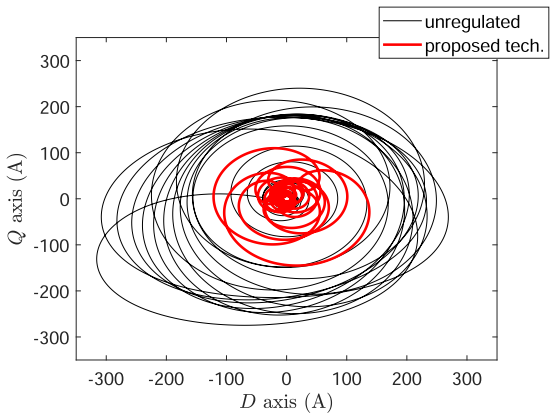

FIGURE 19. Locus of the current vector during the unregulated transition from islanded to grid connected operation – SIMULATION.

FIGURE 21. Photo of the virtual instrument implemented in Labview environment.

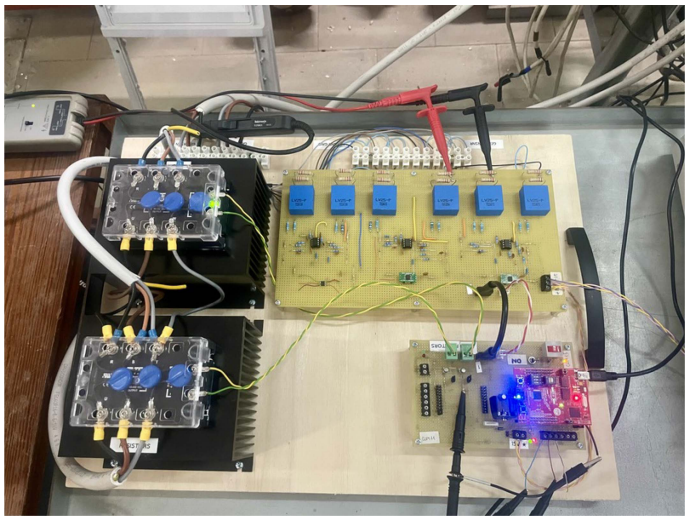

FIGURE 20. Photo of the prototype for the automatic disconnection/reconnection of the SEIG to the power grid.

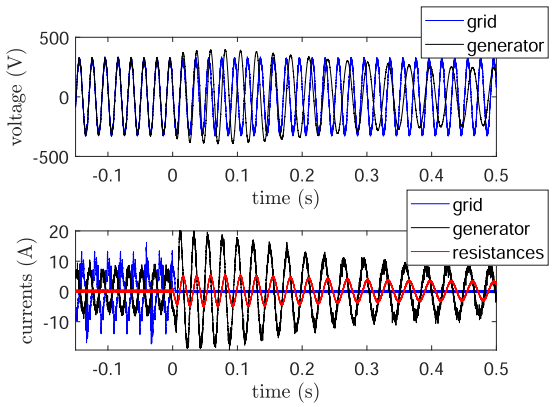

FIGURE 22. IG and grid voltages and IG, load, and grid currents – transition from grid connected to islanded operation.

of a water pumping system and a test stand with the turbine prototype coupled with an IG connected to resistors and capacitors.

A suitable electronic system has been implemented to test the proposed algorithm for the automatic disconnection and reconnection of the IG to the power grid (see Fig. 20). It is composed of a board with LEM voltage sensors model LV25-P for the online measurement of the SEIG and power grid voltages. Furthermore, a TI TMS320F28027 processor has been used to implement the 3/2 transformation, the vector and the scalar products, and the hysteresis comparator highlighted in blue in Fig. 4. Two solid-state contactors model SSR3T-480D25R (turn-ON time: 10 ms; turn-OFF time: 0.1 ms) have been used to connect the IG to either the power grid or the resistor set.

Finally, a virtual instrument (see Fig. 21) has been implemented in Labview environment to monitor in real time all the hydraulic and electrical quantities.

B. EXPERIMENTAL RESULTS

The same kind of tests shown in numerical simulation have been performed experimentally. The first test is the IG to SEIG transient. The IG is initially connected to the power grid and injects an active power of almost 1 kW. At $t = 0\,s$, the IG is disconnected by the power grid and simultaneously connected to the load resistors by commanding the solid-state contactors. Fig. 22 shows the grid and IG voltages, as well as the IG current, the load current, and the current injected into the grid. It shows that, when the IG is connected to the power grid, the IG and grid voltages are superimposed; instead, when the IG transitions to the islanded operation, the IG voltage becomes slightly lower in both amplitude and frequency, as expected. Correspondingly, the IG current presents a transient, with an initial increase and a subsequent decrease when getting closer to the steady-state. The load current, initially null since the load resistance is disconnected from the power grid, becomes not null in islanded operation, as expected. Such a

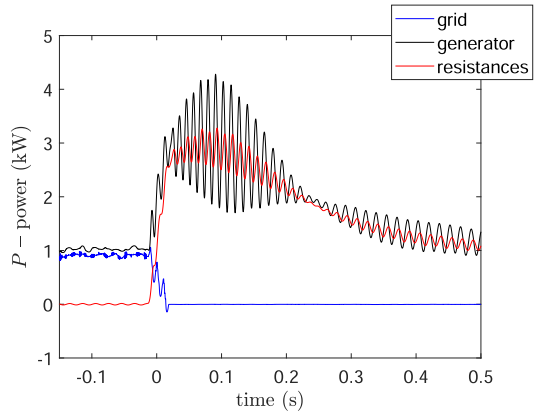

FIGURE 23. IG, load, and grid active powers – transition from grid connected to islanded operation.

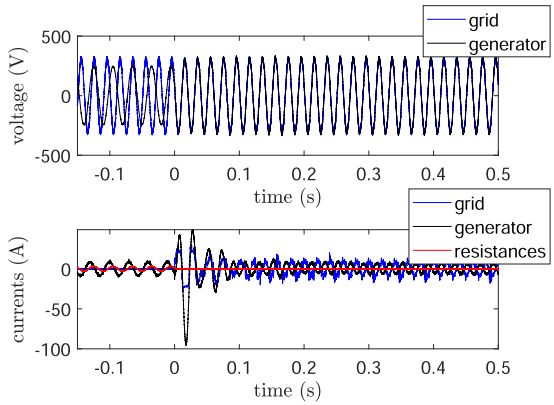

FIGURE 24. IG and grid voltages and IG, load, and grid currents – transition from islanded to grid connected operation.

figure shows that the IG is able to self-excite, as expected based on the design considerations and analysis described in Section V. Fig. 23 shows the active power generated by the IG, the power injected into the grid, and the power delivered to the load resistors. As in the simulated test, the IG power is equal to the power injected into the grid in grid-connected mode and to the load power in islanded operation, as expected. The final IG power is almost 1.1 kW, very close to the initial one. This result is expected, given that the turbine provides almost the same torque and the IG speed slightly varies after the transient, in accordance with the simulation. Overall, the experimental waveforms are very close to those obtained in numerical simulation, thus validating the simulation environment.

The second test is the SEIG to IG transient. Figs. 23 and 24 show the same kinds of waveforms as in the simulation. It can be observed that even the experimental waveforms exhibit a very smooth electromechanical transient. The IG voltage, slightly different from the grid voltage in both amplitude and phase during islanded operation, becomes equal to it in grid-connected operation. The IG current presents a transient with

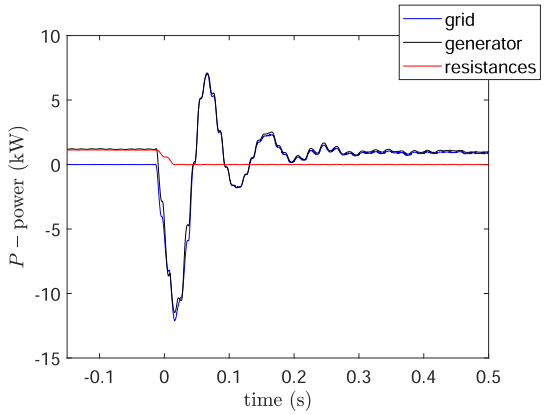

FIGURE 25. IG, load, and grid active powers – transition from islanded to grid connected operation.

an initial increase of the stator current, which rapidly reaches steady state in almost 4 cycles of the fundamental frequency.

The load current, initially null in islanded operation, becomes not null in grid connected operation, being still different from the IG current due to the capacitor current. The active power generated by the IG shows an instantaneous peak of about 13 kW, while it rapidly gets the final steady-state value of 1 kW, as shown in Fig. 25. The above results confirm the goodness of the proposed approach. Unregulated SEIG to IG experimental test have not been performed since the electromechanical transient could have seriously damaged the mechanical system.

IX. CONCLUSION

This article addresses the management of electromechanical transients occurring during disconnection and reconnection to the grid of turbine-driven IGs in hydraulic plants after grid faults. In particular, it deals with the electromechanical stress experienced by an IG during the back transition from the islanded to the grid-connected configuration. After disconnection from the grid, the IG works in islanded mode as an SEIG excited by a capacitor bank and connected to local resistors. Starting from a thorough theoretical analysis of the steady-state and dynamic behavior of the SEIG, as well as from a proper design of the capacitor and load resistance, a low-cost technical solution is proposed to smooth the reconnection transient. Such a solution aims to minimize the peaks and oscillations of the stator currents, electromagnetic torque, and speed occurring when the SEIG is connected back to the power grid by suitably choosing the connection instant. Simulation and experimental results confirm the feasibility of the proposed approach.

APPENDIX
POLYNOMIAL COEFFICIENTS FOR ISLANDED SEIG WORKING FREQUENCIES

The coefficients of the polynomial (1), whose roots are the possible SEIG working frequencies, are the following:

$$A_0 = k_6^2 \left(1 + R_L R_s\right)$$

$$A_1 = -2\left(R_s^2 k_5 k_6 + R_s k_3 k_6 + R_L R_s k_5 k_6\right) - R_L k_3 k_4$$

$$A_2 = R_s^2 k_5^2 + 2R_s^2 k_4 k_6 + k_3^2 + 2R_s k_2 k_6 + 2R_s k_3 k_5 + \\ + X_\sigma^2 k_6^2 + k_1^2 + 2X_\sigma k_1 k_6 + R_L R_s k_5^2 + \\ + 2R_L R_s k_4 k_6 + R_L k_2 k_6 + R_L k_3 k_5$$

$$A_3 = -2\left(R_s^2 k_4 k_5 + k_2 k_3 + R_s k_2 k_5 + R_s k_3 k_4 + \right. \\ \left. + X_\sigma^2 k_5 k_6 + X_\sigma k_1 k_5 + R_L R_s k_4 k_5\right) + \\ - R_L\left(k_2 k_5 + k_3 k_4\right)$$

$$A_4 = \left(R_s k_4 + k_2\right)^2 + X_\sigma^2\left(k_5^2 + 2k_4 k_6\right) + \\ + 2X_\sigma k_1 k_4 + R_L\left(R_s k_4 + k_2 k_4\right)$$

$$A_5 = -2X_\sigma^2 k_4 k_5$$

$$A_6 = X_\sigma^2 k_4^2$$

where

$$k_1 = R_r'^2 X_m', \quad k_2 = R_r' X_m'^2, \quad k_3 = X_m'^2 R_r' V$$

$$k_4 = X_m'^2, \quad k_5 = 2X_m'^2 V, \quad k_6 = R_r'^2 + X_m'^2 V^2.$$

REFERENCES

[1] K. Oikonomou and M. Parvania, "Optimal coordination of water distribution energy flexibility with power systems operation," *IEEE Trans. Smart Grid*, vol. 10, no. 1, pp. 1101–1110, Jan. 2019.

[2] C. Y. Kang, H. Nabipour, H. S. Chua, and C. C. Kang, "Design of battery energy storage system (BESS) with fuzzy control for pico hydro," *Int. J. Elect. Electron. Eng. Telecommun.*, vol. 11, no. 1, pp. 18–23, Jan. 2022.

[3] A. Accetta, M. Luna, M. Pucci, M. Sinagra, and T. Tucciarelli, "A low-cost technique for minimizing the seig electromechanical transient from islanded to grid-connected configuration in hydropower plants," in *Proc. 3 rd Int. Conf. Power Syst. Elect. Technol.*, 2024.

[4] A. Tandon, S. Murthy, and G. J. Berg, "Steady state analysis of capacitor self-excited induction generators," *IEEE Trans. Power App. Syst.*, vol. PAS-103, pp. 612–618, 1984.

[5] S. Rajakaruna and R. Bonert, "A technique for the steady-state analysis of a self-excited induction generator with variable speed," *IEEE Trans. Energy Convers.*, vol. 8, pp. 757–761, Dec. 1993.

[6] C. P. Ion, "A comprehensive overview of single–phase self-excited induction generators," *IEEE Access*, vol. 8, pp. 197420–197430, 2020.

[7] V. Sammartano, M. Sinagra, P. Filianoti, and T. Tucciarelli, "A Banki–Michell turbine for in-line water supply systems," *J. Hydraulic Res.*, vol. 55, no. 5, pp. 686–694, Sep. 2017. [Online]. Available: https://doi.org/10.1080/00221686.2017.1335246

[8] C. Chakraborty, S. Bhadra, and A. Chattopadhyay, "Excitation requirements for stand alone three-phase induction generator," *IEEE Trans. Energy Convers.*, vol. 13, no. 4, pp. 358–365, Dec. 1998.

[9] M. H. Haque, "Determination of NEMA design induction motor parameters from manufacturer data," *IEEE Trans. Energy Convers.*, vol. 23, no. 4, pp. 997–1004, Dec. 2008.

[10] O. Ojo and A. A. Jimoh, "Steady-state and dynamic analyses of isolated self-excited induction generators," *Trans. South Afr. Inst. Elect. Engineers*, vol. 90, pp. 14–19, 1999.

[11] L. Wang and J.-Y. Su, "Dynamic performances of an isolated self-excited induction generator under various loading conditions," *IEEE Trans. Energy Convers.*, vol. 14, pp. 93–100, 1999.

[12] R. Bansal, "Three-phase self-excited induction generators: An overview," *IEEE Trans. Energy Convers.*, vol. 20, pp. 292–299, 2005.

[13] B. Singh, S. Murthy, and S. Gupta, "Transient analysis of self-excited induction generator with electronic load controller (ELC) supplying static and dynamic loads," *IEEE Trans. Ind. Appl.*, vol. 41, pp. 1194–1204, 2005.

[14] M. H. Haque, "A novel method of evaluating performance characteristics of a self-excited induction generator," *IEEE Trans. Energy Convers.*, vol. 24, pp. 358–365, 2009.

[15] M. H. Haque, "Analysis of a self-excited induction generator with P–Q load model," *IEEE Trans. Energy Convers.*, vol. 25, pp. 265–267, 2010.

[16] K. Teng, Z. Lu, J. Long, Y. Wang, and A. P. Roskilly, "Voltage build-up analysis of self-excited induction generator with multi-timescale reduced-order model," *IEEE Access*, vol. 7, pp. 48003–48012, 2019.

[17] O. Kiselychnyk, M. Bodson, and J. Wang, "Linearized state-space model of a self-excited induction generator suitable for the design of voltage controllers," *IEEE Trans. Energy Convers.*, vol. 30, pp. 1310–1320, Dec. 2015.

[18] T. K. Rao, N. Singh, and A. S. Rana, "Fault analysis in power systems comprises of induction machine based DG," in *Proc. Int. Conf. Eng. Innovations Technol.*, Bhopal, India, 2025, pp. 818–823.

[19] U. K. Kalla, B. Singh, and S. S. Murthy, "Modified electronic load controller for constant frequency operation with voltage regulation of small hydro-driven single-phase SEIG," *IEEE Trans. Ind. Appl.*, vol. 52, pp. 2789–2800, 2016.

[20] P. Kumar, U. K. Kalla, N. Bhati, and K. L. Agarwal, "Performance investigation of synchronized three-phase ac chopper-based controller for small hydrogeneration systems," *IEEE Trans. Ind. Appl.*, vol. 58, pp. 2217–2228, 2022.

[21] P. Fedor, D. Perdukova, P. Bernat, L. Stepanec, and V. Fedak, "Modeling of electromagnetic phenomena in small hydroelectric plants," in *Proc. Int. Conf. Elect. Drives Power Electron.*, The High Tatras, Slovakia, 2023, pp. 1–7.

[22] S. Verma, T. R. Chelliah, and R. Kumari, "Black start capability of synchronous and asynchronous hydro generating units," *IEEE Trans. Ind. Appl.*, vol. 61, pp. 5046–5059, 2025.

[23] M. Olivo, A. Vicenzutti, M. Chiandone, G. Sulligoi, and A. Tessarolo, "Generator technologies in Alpine mini hydropower microgrids: A review," in *Proc. 2025 AEIT Int. Ann. Conf.*, Amantea (CS), Italy, 2025, pp. 1–6.

[24] E. Marra and J. Pomilio, "Self-excited induction generator controlled by a vs-pwm bidirectional converter for rural applications," *IEEE Trans. Ind. Appl.*, vol. 35, pp. 877–883, 1999.

[25] S. Rajakaruna and N. N. Maw, "Unregulated performance of an induction generator in an isolated micro hydro power plant," in *Proc. 2005 Int. Power Eng. Conf.*, Singapore, 2005, pp. 1–538.

[26] G. Slemon, "Modelling of induction machines for electric drives," *IEEE Trans. Ind. Appl.*, vol. 25, no. 6, pp. 1126–1131, Nov. 1989.

[27] T. Chan, "Capacitance requirements of self-excited induction generators," *IEEE Trans. Energy Convers.*, vol. 8, no. 2, pp. 304–311, Jun. 1993.